IEEE Access
Multidisciplinary | Rapid Review | Open Access Journal

IEEE POWER & ENERGY SOCIETY SECTION

Received June 21, 2021, accepted July 6, 2021, date of publication July 13, 2021, date of current version July 22, 2021.

Digital Object Identifier 10.1109/ACCESS.2021.3096962

A Supervised Learning Scheme for Evaluating Frequency Nadir and Fast Response Reserve in Ancillary Service Market

HSIN-WEI CHIU, (Student Member, IEEE),
AND LE-REN CHANG-CHIEN, (Senior Member, IEEE)
Department of Electrical Engineering, National Cheng Kung University, East District, Tainan 701, Taiwan

Corresponding author: Le-Ren Chang-Chien (leren@ee.ncku.edu.tw)

This work was supported in part by the Taiwan Power Company under Grant TPC-5460900120.

ABSTRACT Power system operators evaluate the frequency security of the system by predicting the frequency nadir, which is assumed to indicate the impact of a sudden loss of a generating resource. Recently, frequency nadir prediction has become more challenging because renewables have penetrated and significantly changed the generation portfolio within the system. Conventionally, the frequency nadir is determined using a frequency response model where the features—load damping, system inertia, and effective governor response—are assumed to be known. However, these key features are not easily obtained in a power system that continuously changes during daily operation. This study proposes a supervised learning scheme that traces these key features. It also proposes a new feature—the power gap rate—that better reflects the influence of the load on the system frequency than that of the load damping. Feature importance recognition and the construction of a frequency nadir model (FNM) are realized using the proposed supervised learning scheme. The proposed FNM achieved 54% higher accuracy than the conventional method. Finally, the FNM is implemented in a planning process that quantifies the capacity of the fast responsive reserve (FRR). In two renewable penetration cases, the proposed FRR procurement successfully secured the frequency nadir above the security criterion.

INDEX TERMS Frequency nadir, fast responsive reserve, primary frequency response, supervised learning.

I. INTRODUCTION

Operating reserves (ORs) are deployed during a frequency disturbance in a power system. Balancing authorities (BAs) usually acquire the OR from ancillary service markets for different demands and applications [1]. Depending on the need for frequency support, an OR can be event-driven or non-event driven. The non-event driven OR maintains frequency stability in cases of continuous load variations or inaccurate day-ahead load forecasts [2], whereas event-driven OR intercepts and restores the falling runaway frequency during a contingent event [3]. Unless the frequency decline is successfully intercepted and restored above the specified threshold, unexpected load shedding could be triggered. Inertia-driven conventional units are now increasingly being replaced by noninertia-driven renewables, thereby increasing the risk of frequency fall. In this situation, a fast response reserve (FRR) that responds within one second is urgently needed [4]. Several BAs, such as the Electric Reliability Council of Texas, the Australian Energy Market Operator, and the Taiwan Power Company (TPC), are developing FRR commodities in the ancillary service market [5]–[7]. The rising demand for FRRs has also increased interest in FRR-related problems [8]–[11]. Conventionally, FRRs are evaluated using frequency nadir prediction in frequency response models (FRMs) [12]–[14]. However, the load damping of a FRM changes with load conditions in a power system [15]–[17]. Moreover, the time-varying response of the speed droop governor in a generator unit strongly affects the unit's ability to support a frequency disturbance event. These features considerably affect the efficacy of frequency nadir prediction. Most commonly, a FRM is improved via statistical analysis under different operating conditions. Wu and Chen evaluated the recovery reserve using the frequency nadir after dividing the load–frequency sensitivity feature (load damping) into different categories [18]. Chang *et al.* proposed the ratio of

The associate editor coordinating the review of this manuscript and approving it for publication was Emilio Barocio.

generation deficiency to frequency decline and then predicted the post-incident frequency nadir using a decision tree [19]. Wu *et al.* constructed an FRM by performing multiple linear regression analysis on the historical records collected using a phasor measurement unit [20]. Moreover, frequency nadir can be predicted using nondeterministic models. Zografos *et al.* predicted the frequency nadir using a neural network (NN) by providing the frequency, inertia constant, initial disturbance, and voltage dynamics as inputs [21]. Although statistical analyses and NN models can predict the frequency fall during a disturbance, they require amassed historical data, which are occasionally insufficient for model construction. To obtain a sufficient database, the collected data must be traced over numerous previous years, which may lead to the loss of current change trends such as increasing renewable penetration.

Frequency nadir prediction faces one of two main challenges: either the model features are difficult to obtain in the dynamic system state or the model features exert different influences on the actual system. To solve the aforementioned problems, we should understand the importance of the features relating the frequency nadir. When input with the most influential features, the model will better reflect the actual response under different operating conditions. Recently, several machine learning algorithms have delivered satisfactory performance in power system applications [22]–[25]. In the present research, a supervised learning algorithm is embedded in a FRM for frequency nadir prediction during contingent events. Models built using supervised learning can be continuously revised and effectively fitted with labeled contingent event data (label: frequency nadir) to evaluate the model performance and ensure its accuracy. The proposed supervised learning-based method can better estimate the frequency disturbance trend; thus, the predicted frequency nadir will be more accurate than the traditional method. The main contributions of this research are summarized below.

(1) A new system feature of the FRM, called the power gap rate (PGR), is proposed using supervised learning. The PGR reflects load damping and system inertia, which helps predict the frequency nadir after a system disturbance.

(2) The primary frequency responses (PFR) of various fuel-type units are assessed using a linear regression method. The PFR is useful for evaluating the frequency nadir during frequency disturbance events.

(3) The supervised learning procedure for the model construction, including feature selection, feature modeling, and model validation, is demonstrated.

(4) The proposed FRM can portray different operating cases such as different renewable penetrations into the power system. The proposed model forecasts the likely challenges faced by system operators.

The remainder of this paper is organized as follows. Section II describes the planning and estimation process of the FRR capacity. Section III introduces the conventional methods to assess the primary frequency response and load damping and discusses their limitations to the frequency nadir prediction. Section IV presents a key feature (PGR) obtained by analyzing the actual contingency events. Section V constructs the FNM using the supervised learning algorithm and compares the results of the proposed and the other methods. Section VI demonstrates the findings of the proposed FRM in two case studies. Section VII presents concluding remarks and suggests avenues for future research.

II. PLANNING FOR FRR CAPACITY

Estimating the frequency nadir after a unit trip is essential in power systems. If the frequency nadir is excessively low, the system will trigger underfrequency load shedding (UFLS) to quickly restore the power balance [26]. The most effective approach for preventing a UFLS trigger is reducing the power gap during the arresting period. This can be achieved using the frequency response reserve such as a battery energy storage system (BESS) or demand response (DR) that can be procured from the ancillary service market [27], [28]. However, FRR procurement is challenged by the different responses and time delays of various generating resources. Understanding the system operation at the planning stage would improve the preparation of FRR. Fig. 1 shows the day-ahead FRR capacity planning process including timeline. The timeline depends on the electricity market in Taiwan. Based on the day-ahead hourly information (after 16:00), i.e., load forecasts, renewable energy forecasts, and unit scheduling results, we can evaluate the degree of frequency fall during a unit trip and the amount of additional FRR that will arrest further frequency fall. The detailed procedure for calculating the additional FRR capacity is described in Section V. D. The evaluation and adjustment of the additional FRR can be iterated until the frequency nadir is recovered above the criterion.

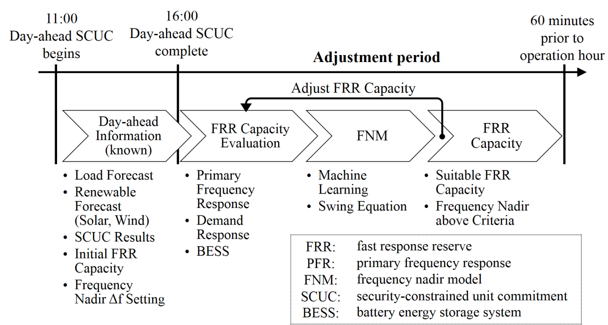

FIGURE 1. Flowchart of FRR capacity planning.

III. ASSESSMENT OF THE PFR AND D VALUE

A. PRIMARY FREQUENCY RESPONSE (PFR)

Most conventional generating units in power systems are equipped with the PFR function (also known as the governor response). The PFR provides a fast power-output adjustment to the frequency variation. The droop setting of the PFR is formulated using (1):

$$Droop = \frac{\Delta f}{\Delta P} = \frac{f - f_0}{P - P_0}. \tag{1}$$

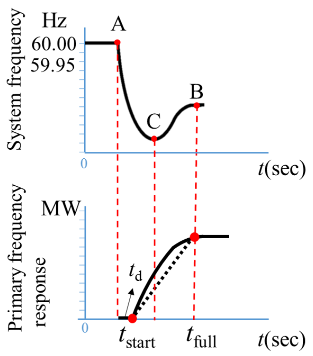

FIGURE 2. Primary frequency response to the system frequency.

The maximum droop value (%) differs among unit types. For example, the droop is 4%, 5%, 4.5%, and 3% in gas-fired combined cycle units, coal-fired steam turbines, oil-fired/gas-fired steam turbines, and hydro units, respectively. We additionally found that the PFR does not fully react at the time point of the frequency nadir. Fig. 2 shows the time delay (t_d) between the system incident point (point A) and PFR activation (solid black line). The full PFR response was reached not at point C (the frequency nadir) but at a later point B. If the PFR of the online unit is directly calculated using the nominal values, the result is overestimated and the predicted frequency dip is smaller than the actual dip. Therefore, the effective PFR must be evaluated in real cases.

We analyzed the PFR responses of online units using 82 contingency events of the TPC system collected during the past seven years (2013–2019). The effective PFR is calculated using (2) for different fuel-type units (Fig. 3):

$$PFR_{(\text{pu})} = \frac{\left(P_{\text{C-point}} - P_{\text{A-point}}\right)}{P_{\max}}. \tag{2}$$

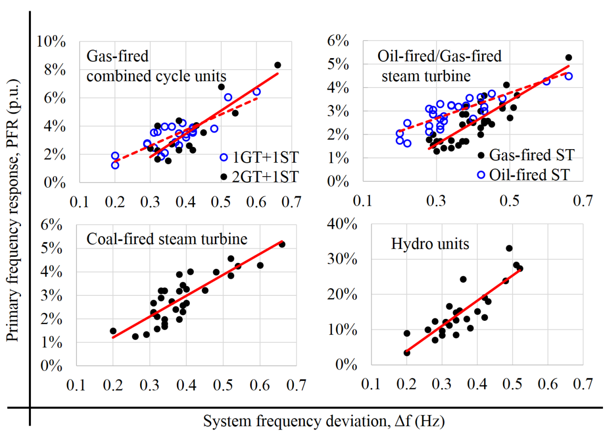

FIGURE 3. Effective PFRs as a function of the system frequency deviation.

The frequency fall-off curve was initially steep, and the decline in frequency was linearly related to the unit response. Thus, the PFR was described using a simple linear equation (3) and the closeness of the data trend to the linear equation was evaluated by employing the R^2 measure [29] calculated using (4)–(6), where $PFR_{i(pu)}$ is the actual PFR of the i^{th} unit in p.u., $PFR^*_{i(pu)}$ is the predicted PFR of the i^{th} unit in p.u, and $\overline{PFR}_{(pu)}$ is the mean value of all PFRs in p.u. for the same fuel type. In (3), the constant a represents the droop slope and the constant b represents a dead-band for activating the response. Finally, the available PFR response is calculated using the unit megawatt rating and (3), which is shown in (7).

$$PFR_{(\text{pu})} = a\Delta f + b, \tag{3}$$

$$SSE = \sum_{i=1}^{n} \left(PFR_{i(\text{pu})} - PFR^*_{i(\text{pu})}\right)^2, \tag{4}$$

$$SST = \sum_{i=1}^{n} \left(PFR_{i(\text{pu})} - \overline{PFR}_{(\text{pu})}\right)^2, \tag{5}$$

$$R^2 = 1 - \frac{SSE}{SST}, \tag{6}$$

$$PFR = P_{\max} * PFR_{(\text{pu})} = P_{\max} * (a\Delta f + b). \tag{7}$$

The PFR models and R^2 fittings for each fuel-type unit are presented shown in Table 1. All R^2 values exceeded 0.7, implying that the post-incident frequency change Δf is highly correlated with the PFR response. The speed droop settings significantly differed from the nominal values, possibly because the actual system exhibits an inherent time delay and incomplete governor response.

TABLE 1. Linear regression model of PFR for all types of units.

	Linear Regression Model	R^2
Gas-fired combined cycle units (1GT + 1ST)	$PFR_{(pu)} = 0.112 \times \Delta f - 0.008$	0.72
Gas-fired combined cycle units (2GT + 1ST)	$PFR_{(pu)} = 0.165 \times \Delta f - 0.031$	0.71
Gas-fired steam turbine	$PFR_{(pu)} = 0.092 \times \Delta f - 0.012$	0.72
Oil-fired steam turbine	$PFR_{(pu)} = 0.054 \times \Delta f - 0.011$	0.74
Coal-fired steam turbine	$PFR_{(pu)} = 0.089 \times \Delta f - 0.006$	0.72
Hydro units	$PFR_{(pu)} = 0.713 \times \Delta f - 0.103$	0.75

B. CONVENTIONAL ASSESSMENT OF THE LOAD DAMPING (D VALUE) USING THE SWING EQUATION

To procure a sufficient FRR for frequency security, we must first evaluate the frequency nadir assuming that the system suddenly loses its largest generation unit. Conventional FRMs are based on the following swing equation [12]–[14]:

$$\frac{2H}{f}\frac{df}{dt} = \frac{P_{outage}}{S_{base}} - \frac{PFR}{S_{base}} - D\frac{\Delta f}{f}, \tag{8}$$

where P_{outage} is the generation loss, PFR is the PFR support from online units, and D is the load damping.

After a unit trip, the system frequency will rapidly decline to the nadir point. Evidently, the frequency change (i.e., the first derivative of f) is zero at the nadir point. Equation (8) can then be rewritten as

$$0 = \frac{P_{outage}}{S_{base}} - \frac{PFR}{S_{base}} - D\frac{\Delta f}{f}. \tag{9}$$

The information regarding PFR, Δf, P_{outage}, and the installed capacity of all online units (S_{base}) in (9) can be obtained using the contingency event of each unit. The unknown load damping D can then be estimated as

$$D = \frac{f}{\Delta f}\left(\frac{P_{outage}}{S_{base}} - \frac{PFR}{S_{base}}\right) pu. \tag{10}$$

In power systems, D is quite complicated because it depends on the load type and time characteristics [13], [15]–[17]. In this study, the D value was estimated from 82 contingency events and separated into three operation-shift intervals (first shift: 00:00–09:00, second shift: 09:00–17:00, and third shift: 17:00–24:00). As shown in the box plot (Fig. 4), the D values were scattered during the first shift period and concentrated during the third shift period. The average D values in the first, second, and third shifts were 1.46, 1.27, and 1.41, respectively.

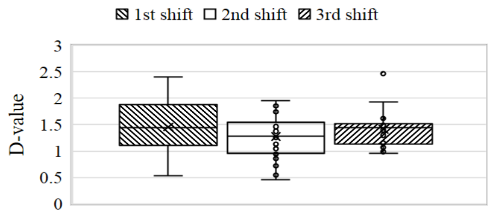

FIGURE 4. D values and ranges during three operation shifts.

After calculating the D value in each shift interval, Δf can be calculated using (9). The frequency nadir is then obtained as

$$f_{nadir} = f_0 - \Delta f. \tag{11}$$

The predicted f_{nadir} was compared with the actual f_{nadir} in the 82 contingency events. The root mean square errors (RMSEs) in the first, second, and third shift periods were 0.15, 0.12, and 0.11 Hz, respectively. The poorer result in the first shift period compared with the other periods can be attributed to the scattered D values in that period, as shown in Fig. 4. This result implies a limit on the statistical D value.

If the FRR is provided using DR and BESS, we can calculate the BESS term $FRR_{DR+BESS}$ using (12), which assumes that Δf is the maximum allowable frequency deviation:

$$FRR_{DR+BESS} = P_{outage} - PFR - D\frac{\Delta f}{f}S_{base}. \tag{12}$$

IV. NEW FINDINGS FOR ASSESSING FREQUENCY DEVIATIONS

As shown in Fig. 4, the D value varies with the load composition and time and an accurate estimation is difficult. According to the swing equation, as shown in (8), the frequency nadir can be evaluated by predicting Δf. To predict Δf, we must know the values of P_{outage}, PFR, D (load damping), H (inertia constant), and df/dt (so called ROCOF). Predicting the exact future value of ROCOF is challenging. To overcome this obstacle, this study identifies the importance of each feature in supervised learning (see next section). Moreover, we proposed the PGR defined as the difference between the generation loss (unit trip) minus the contribution of the PFR. The PGR represents the composite term of load damping and inertial effect in the swing equation, which more accurately traces the frequency nadir than the D value.

An actual contingency event is shown in Fig. 5. The dashed black line represents the system frequency, the solid blue line represents the tripped unit capacity, and the solid red line represents the power gap (ΔP). In this actual event, 980 MW of the unit tripped at point A. Within 12 s during the frequency decline from A to C, the system frequency was first affected by the system inertia and load damping and affected by the partial PFR. However, the power gap at point C was still 560 MW because the PFR at point C was only 420 MW. To account for the effect of load damping and system inertia on the frequency nadir, the PGR was calculated as the percentage of the power gap to the total net load before the event, as shown in (14). In the TPC system, the industrial load accounts for 60%–70% of the total system load. The industrial load involves many rotary motors. Therefore, the larger (smaller) the total net load before the event, the larger (smaller) the system inertia and load damping. The PFR continued to increase until the online generating units fully delivered the PFR. The frequency eventually settled at point B.

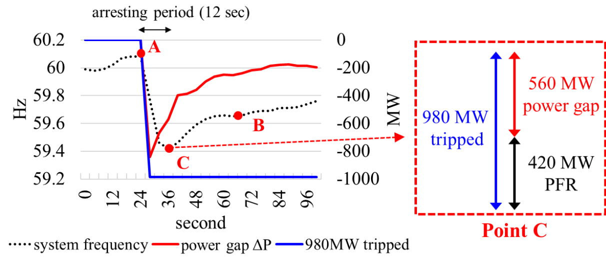

FIGURE 5. Demonstration of the power gap in a real system.

$$PowerGap = P_{outage} - PFR, \tag{13}$$

$$PGR = \frac{PowerGap}{NetLoad}. \tag{14}$$

Figs. 6 and 7 plot the frequency deviation Δf versus $D^*\left(\Delta f/f\right)$ and PGR, respectively. The R^2 values in Figs. 6 and 7 were 0.56 and 0.76, respectively, confirming that PGR is more strongly related to Δf than the load damping in the swing equation.

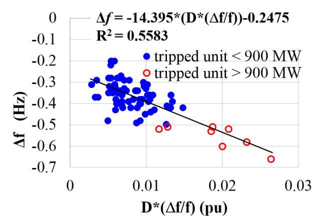

FIGURE 6. Relationship between D*(Δf/f) and frequency deviation (Δ*f*).

The PGR was found to be the most effective approach for evaluating the synthetic effect of load damping and inertial responses on the frequency nadir. In the past, the load damping and system inertia could not be fully grasped at the time of prediction because these values continued to vary. The conventional technique for predicting the frequency nadir is the use of the statistical values of the load damping and system inertia. This approach could result in a large prediction error if the load damping and system inertia values were not estimated well. The PGR helps the supervised learning

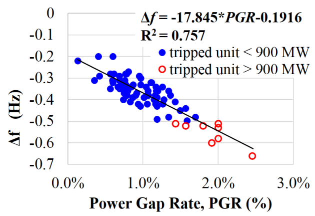

FIGURE 7. Relationship between power gap rate (PGR) and frequency deviation (Δf).

algorithm trace the system behavior trend, achieving a better estimation of the frequency nadir prediction than the conventional technique.

V. SUPERVISED LEARNING FOR FEATURE ANALYSIS

Generally, the load-side frequency response is a complicated part of the power system described using a multivariate and time-dependent function that cannot be easily grasped using the conventional linear system approach. Herein, we attempted to analyze the importance of frequency nadir features and to construct a FNM using the supervised learning algorithm. The procedure of the modeling process is shown in Fig. 8.

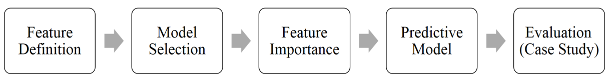

FIGURE 8. Construction process of the FNM based on supervised learning.

A. FEATURE DEFINITION

After a comprehensive discussion with the system operators, we identified several influencing features from the load side that may impact the frequency response. The influential features were divided into two major categories: one related to the operating period and the other related to the physical system.

The operating period-related features were season, working day/holiday, and the three shift intervals. Moreover, the physical system-related features were load ramp status, net load, lumped generator inertia (gen-inertia), PFR, and PGR.

To compare the influence of the features, these features were grouped into three sets: Set A containing all time-related and system-related features excluding gen-inertia, PFR and PGR, Set B containing the same features as Set A as well as the gen-inertia, and Set C containing all features including PFR and PGR.

B. MODEL SELECTION

Many algorithms for machine learning techniques are developed in scikit-learn on the Python platform [30]. Traditional machine learning methodologies include linear regression, Bayesian ridge, support vector regression, and decision trees. The newly developed tree-based ensemble learning methods are random forest, gradient boosting decision tree (GBDT), and Xgboost. Long short-term memory (LSTM) is a representative NN deep learning framework [31]–[34]. Generally, NN-based algorithms perform better with a large amount of training data. Even though a deep learning NN shows the optimal internal tuning capability for model hyperparameters, data independency is still instrumental in model tuning. Our tests show that data adequacy is crucial for the NN-based model accuracy. The relevant results are provided in Section V. D. Therefore, we selected tree-based supervised learning rather than deep learning NN algorithms. Tree-based ensemble learning combines multiple weak classifiers (i.e., regression tree) into one strong classifier, which can be bagged for parallel generation and boosted for sequential generation [35]. Experience has shown that boosting models such as GBDT (2001) and Xgboost (2017) are superior to bagging models such as the random forest (1997) [35]. In the boosting method, the weak classifier reduces the residual error along the gradient direction; in other words, a weak classifier with a smaller error is weighted more heavily than one with a larger error until the last model is obtained. Xgboost avoids model overfitting and accelerates the convergence speed of the model fitting [33]. Xgboost also shows promising performance in Kaggle machine learning competitions, which honor the best machine learning algorithms [36]. Hence, we employed Xgboost as the feature importance analyzer for our FNM, which we refer to as FNMXGB. The algorithm proceeds as follows.

The objective function of Xgboost adds regularization to the loss function as

$$\hat{L}^{(t)} \cong \sum\nolimits_{i=1}^{n} l\left(y_i, \hat{y}_i\right) + \sum\nolimits_{k=1}^{t} \Omega\left(f_k\right), \tag{15}$$

where $l\left(y_i, \hat{y}_i\right)$ is the loss function and $\Omega\left(f_k\right)$ is the regularization that penalizes the complexity of each regression tree.

The regularization depends on the number of leaf nodes of tree T and the sum of squares of the L2 modes of the output scores on each leaf node ω:

$$\Omega\left(f_k\right) = \gamma T + \frac{1}{2}\lambda \left\|\omega\right\|^2. \tag{16}$$

After the t-th iteration, the prediction of the model equals the prediction of the previous model and the prediction of the tth tree, as shown in (17):

$$\hat{y}_i = \hat{y}_i^{(t-1)} + f_t\left(x_i\right). \tag{17}$$

Therefore, the objective function (15) can be written as (18). Equation (19) is obtained as the second-order Taylor's expansion of (18) at $\hat{y}_i^{(t-1)}$ with the constant term removed.

$$\hat{L}^{(t)} = \sum\nolimits_{i=1}^{n} l\left(y_i, \hat{y}_i^{(t-1)} + f_t\left(x_i\right)\right) + \sum\nolimits_{k=1}^{t} \Omega\left(f_k\right), \tag{18}$$

$$\hat{L}^{(t)} \cong \sum\nolimits_{i=1}^{n} \left[g_i f_t(x_i) + \frac{1}{2} h_i \left(f_t(x_i)\right)^2\right] + \sum\nolimits_{k=1}^{t} \Omega\left(f_k\right), \tag{19}$$

where $g_i = \partial_{\hat{y}_i^{(t-1)}} l\left(y_i, \hat{y}_i^{(t-1)}\right)$ and $h_i = \partial^2_{\hat{y}_i^{(t-1)}} l\left(y_i, \hat{y}_i^{(t-1)}\right)$.

Expressing the target function in terms of the leaf node ω_j, we obtain

$$\hat{L}^{(t)} = \sum\nolimits_{j=1}^{T} \left[G_j \omega_j + \frac{1}{2}\left(H_i + \lambda\right)\omega_j^2\right] + \gamma T. \tag{20}$$

Finally, the minimum loss (21) is obtained by substituting the optimal prediction score $\omega_j^* = -\frac{G_j}{H_j+\lambda}$ of each leaf node in (20).

$$\hat{L}^* = -\frac{1}{2}\sum_{j=1}^{T}\left(\frac{G_j^2}{H_j+\lambda}\right) + \gamma T. \tag{21}$$

In our case, the feature sets presented in Table 2 are the input $x's$ of (17), where $y's$ are the output representing the frequency deviation Δf. Finally, the predicted frequency nadir can be obtained using (11).

TABLE 2. Features affecting the frequency nadir.

Features		Feature Set A	Feature Set B	Feature Set C
Time related		Season		
		WorkingDay		
		ShiftInterval		
System related		Load Ramp Status		
		Net load		
		-	Gen-inertia	Gen-inertia
		-	-	PFR
		-	-	PGR
Goal		FreqDev (Δf)		

C. FEATURE IMPORTANCE

This subsection determines the importance of the frequency nadir features contained in the three sets presented in Table 2. The 82 contingency events were divided into training (70%) and testing (30%) sets. The model was trained using the five-fold cross-validation technique of the frequency nadir features. In this process, the training set was divided into five folds, and the training set was executed five times. During each execution, the accuracy of the model was evaluated on one fold (20%) of the training set to avoid model overfitting. The optimal hyperparameters were tuned with a range using a grid search method [30]. The hyperparameters used to construct the three FNMXGB models are listed in Table 3. The RMSEs of the frequency nadir prediction are also shown in Table 3.

TABLE 3. Hyperparameter settings and RMSEs of Xgboost in each model.

	Feature Set A	Feature Set B	Feature Set C
max_depth:[1,10]	3	3	5
n_estimator:[50,100]	50	70	60
learning_rate:[0.01,0.2]	0.1	0.1	0.1
min_child_weight:[0,10]	6	7	6
colsample_bytree:[0.5,0.9]	0.6	0.8	0.8
gamma	0	0	0
reg_alpha	0	0	0
reg_lambda	1	1	1
RMSE (Hz)	0.072	0.068	0.051

In the three datasets, the frequency nadir accuracy depended on the feature sets. The RMSEs of Sets A, B, and C were 0.072, 0.068, and 0.051 Hz, respectively. In Sets A and B, gen-inertia was an unimportant influence of frequency nadir, consistent with (9) (the system inertia was ignored in the conventional approach). The frequency nadir was more accurately determined in Set C than in Set A and B and was far superior to the frequency nadir derived using the swing equation (Section III).

The importance of each feature with respect to the frequency nadir was determined by counting the nodes of each tree in the tree-based training model. For more details, readers can refer to a study by Chen *et al.* [33]. Fig. 9 ranks the features based on their importance. The PGR contributed close to 50% of the results, distantly followed by Net Load, PFR, and gen-inertia. The ranking validates the influential effect of the PGR on the frequency nadir prediction. Additionally, this ranking is consistent with the load structure of the TPC system. In the TPC system, the industrial load accounts for 60%–70% of the total system load. Among the industrial load, the industrial motors account for a high percentage. This is the reason the ranking of the net load is higher than that of PFR and gen-inertia in the feature importance analysis. In the UFLS calculation, only the initial rate of frequency decline is unaffected by the load damping. When the frequency decline is more evident, the influence of the load damping should not be ignored [27].

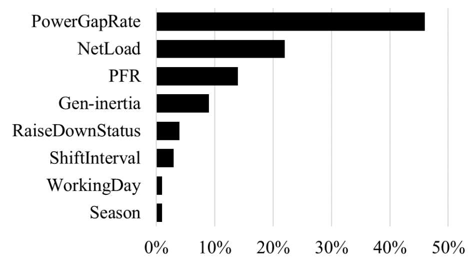

FIGURE 9. Importance ranking of frequency decline features.

As expected, the effects of the time-related features were less significant. Because the top four features collectively accounted for 90% of the result, they were selected as the key features for the FNM prediction. When the FNMXGB-type FNM selected the four key features, the RMSE of the frequency nadir only marginally increased (from 0.051 to 0.054 Hz). Maintaining the important features can reduce the data collection process and data-processing efforts without increasing the error beyond the allowable range.

D. SUPERVISED LEARNING MODEL AND COMPARISON WITH OTHER MODELS

To gauge the performances of different model frameworks, we constructed the frequency nadir models using the traditional swing equation (FNMSE), NN-based LSTM (FNMLSTM), and tree-based Xgboost (FNMXGB). All models were required to evaluate the frequency deviation from the largest unit trip. Their prediction flowcharts were similar but not identical. Note that the models differed mainly by their utilized key features and model cores. FNMSE predicted Δf using the installed capacity of the online units (S_{base}) and statistical load damping. Alternatively, FNMLSTM and

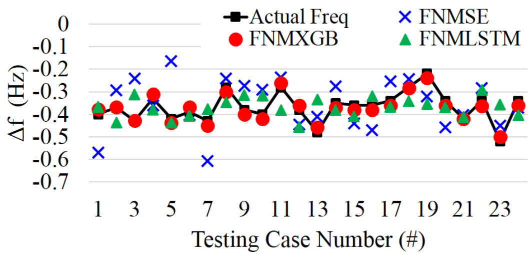

FIGURE 10. Frequency deviations among 24 testing cases using the three FNM models.

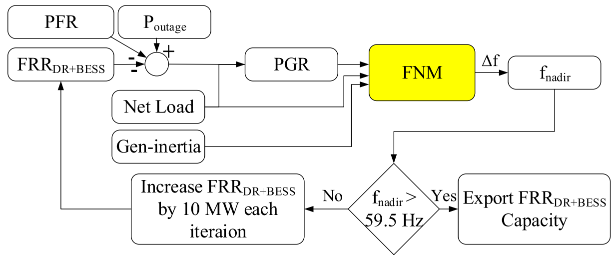

FIGURE 11. FNM flowchart to predict Δf and $FRR_{DR+BESS}$.

TABLE 4. RMSEs of 24 testing cases using the three FNM models.

	Average RMSE (Hz)	Improvement (%)
FNMSE	0.11	-
FNMLSTM	0.08	27%
FNMXGB	0.05	54%

FNMXGB predicted Δf using the PFR, PGR, total net load, and gen-inertia. For a fair comparison among different supervised learning algorithms, our test adopted the same five-fold cross-validation technique using the same datasets, i.e., the same training and testing samples.

Overall, 24 cases were randomly selected from the 82 events for model validation. The prediction results of the three models are depicted in Fig. 10. In this figure, the actual frequency deviations (black squares) and the predicted results of FNMSE (blue crosses; see Section IV), FNMLSTM (green triangles), and FNMXGB (red circles; see Section V) are shown. The frequency deviations among the 24 cases ranged from −0.2 to −0.58 Hz. The training data cover most of the possible cases. The RMSEs of the three models and their relative improvements are presented in Table 4. FNMXGB clearly outperformed the other models. FNMSE performed poorly, probably because the D values were less accurately estimated than in the other models. The PGR best reflected the net load with the load damping, which effectively improved the accuracy of FNM. Although FNMLSTM adopted a deep learning approach to tune the model features, it could not compete with FNMXGB.

Once the frequency nadir was predicted, the day-ahead FRR requirements in each operating hour were calculated following the flowchart in Fig. 1. Based on the day-ahead unit commitment results, the setpoint of each unit was determined and the total PFR capacities of the scheduled units were calculated using the PFR models listed in Table 1, derived from (7). A low PFR can induce a large PGR, thereby reducing the frequency nadir to below the preset level. Therefore, additional DR and BESS ($FRR_{DR+BESS}$) must be procured. The additional $FRR_{DR+BESS}$ is procured to ensure that the frequency nadir is above 59.5 Hz. As shown in Fig. 11, the additional $FRR_{DR+BESS}$ value is calculated iteratively within the loop containing the FNM. Note that the iteration process is necessary because different quantities of the injected FRR affect the frequency deviation and the frequency deviation subsequently affects the PFR and PGR responses. The different PFR and PGR responses will then affect the frequency deviation again. Our test shows that the accuracy of the frequency nadir prediction is considerably better than that of the definite method (FNMSE).

Fig. 12 shows an actual contingency event and the simulated result from Power System Simulator for EngineeringPSS/E. The solid black line represents the historical frequency curve after a 980-MW unit tripped. The frequency nadir was at 59.42 Hz owing to insufficient PFR during the midnight operation (the first shift). The dashed blue line represents the simulated frequency curve after the injection of the $FRR_{DR+BESS}$. When the frequency passed the 59.8-Hz threshold, the 220-MW $FRR_{DR+BESS}$ was injected into the system, stopping the frequency fall at 59.51 Hz. The trace of the frequency curve validates the effectiveness of the proposed method.

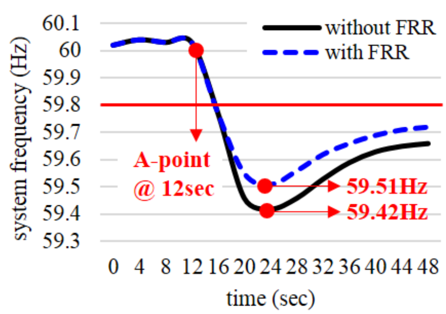

FIGURE 12. Frequency curve comparison with and without FRR injection.

E. DATA CHARACTERISTICS AND TRAINING ADEQUACY

In this test, 82 contingency data over the past seven years were collected for FNM modeling and analysis. FNM was trained using the five-fold cross-validation technique. Within the training data, the frequency deviations ranged from −0.2 to −0.58 Hz, which covers most of the possible cases. The RMSE of the test data was 0.05 Hz, indicating the sufficiency of the training data.

To closely trace the frequency behavior, the FNM needs the following data: the information of the entire system (date, time, system frequency, system load, and net load); tripped unit information (trip time, trip unit, and trip capacity), the megawatt output information of the online unit during the frequency disturbance event; and characteristic information of the online units (fuel type, unit capacity, maximum output, minimum output, unit inertia, and the configuration of the combined cycle unit). The system data were obtained using the energy management system of TPC, which shows the sampling rate of 2 s.

According to TPC's contingency events, the frequency decline required 8 to 12 s from the initial fall to the nadir point. To improve the evaluation accuracy, we found that frequency measurement with less than 60 ms/sample could serve our need. Therefore, we adopted the frequency data retrieved from the TPC's phasor measurement unit with a sampling rate of 10 ms/sample.

VI. CASE STUDY

In 2019, the total installed capacity of TPC's system was 56 GW and the generation mix consisted of approximately 75% fossil fuels, 8% nuclear, 5% pumped storage hydro, 4% cascading hydro, 7% photovoltaic (PV) generation, and 1% other renewable resources [25]. By 2025, the TPC system will reach 14 GW of PV penetration in the system during the peak sunshine hours (peak load is approximately 40 GW). Therefore, the renewable energy source (RES) penetration can reach 35%, a level not reached in TPC history. Therefore, the TPC system operators could receive information whether the frequency nadir can be secured during the daily operating periods.

Two case studies are investigated in this study. Case I is a real operation case with a low penetration of RESs, and Case II shows a high penetration of RES, accounting for 35% of the total installed capacity. The frequency nadir prediction and FRR procurement were performed as shown in Fig. 11. The largest unit trip in both cases was 980 MW. The frequency nadir was estimated using the proposed FNM (FNMXGB) and used for calculating the additional $FRR_{DR+BESS}$ to be purchased from the ancillary service market.

A. LOW RES PENETRATION CASE

The day-ahead scheduling results per hour are shown in Fig. 13. From these scheduling results, the setpoint of each generating unit is clearly known. The corresponding PFR can be estimated using the models presented in Table 1. In the

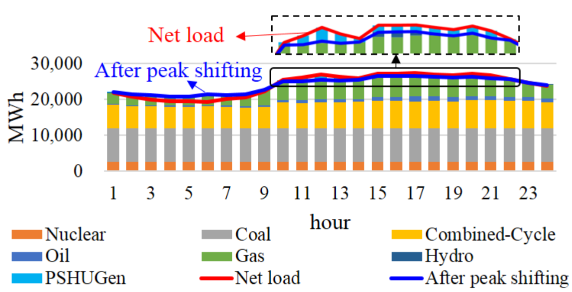

FIGURE 13. Day-ahead scheduling results with low RES penetration.

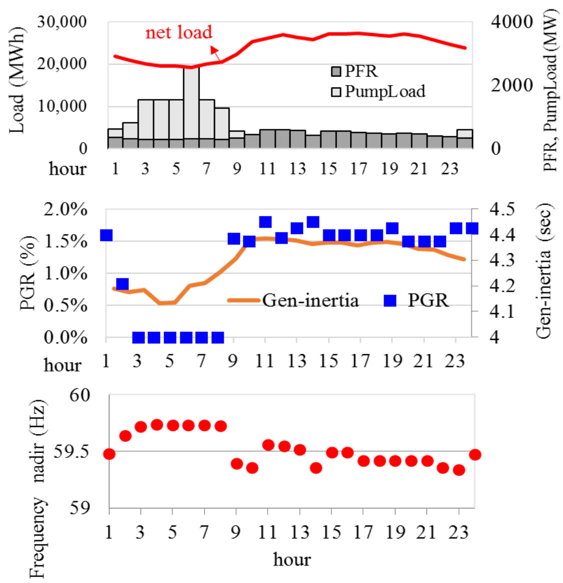

FIGURE 14. Loads, PFRs, PGRs, gen-inertias, and nadir frequencies in each hour estimated using the proposed FNM.

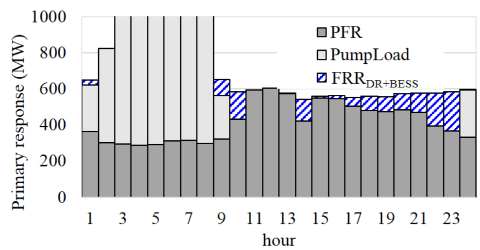

FIGURE 15. FRR capacities at the safe frequency nadir.

TPC system, pumped storage hydro units with a 2602-MW capacity are available for peak load shifting. Fig. 13 shows two load lines representing the net loads with and without peak load shifting.

Fig. 14 presents the day-ahead scheduling results of the net load, PumpLoad (pumping load), Gen-inertia, PFR, PGR, and frequency nadir estimated using the proposed FNMXGB. When the system inertia was excessively low during the off-peak hours, the UC scheduled the pumping load to sufficiently supply the FRR and the frequency nadir remained above the requisite 59.5 Hz during the 980-MW unit trip. However, during the load ramping period (load rise or fall), the PFR deficit increased the PGR value by more than 1.6% and the frequency nadir fell below 59.5 Hz. This situation was observed in nine periods.

Additional $FRR_{DR+BESS}$ was prepared to secure the nine anomalous periods. The $FRR_{DR+BESS}$ quantities procured per hour are shown in Fig. 15. The day-ahead UC results show that most scheduled additional FRR purchases were required during the semipeak periods. Overall, the FRR and PFR range in each period was approximately 550–600 MW. The additional $\mathrm{FRR}_{\mathrm{DR+BESS}}$ capacity to be purchased over 24 h was 1220 MWh.

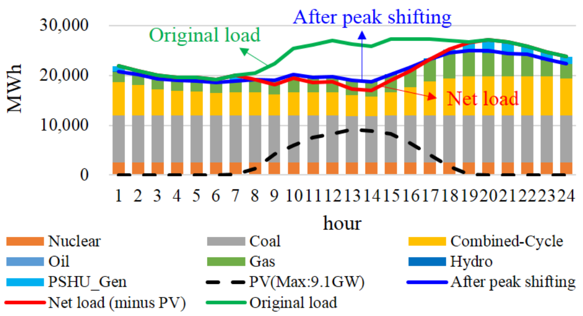

FIGURE 16. Day-ahead scheduling results in a system with high PV penetration.

B. HIGH PV PENETRATION CASE

Case II was investigated under a similar load as Case I but was highly penetrated by PVs (installed capacity = 13 GW). The UC scheduling result is shown in Fig. 16. The peak load in Case II shifted from 15:00 to 20:00. Evidently, the high penetration of the RES significantly changed the UC scheduling results.

Fig. 17 plots the net load, PumpLoad (pumping load), PFR estimated using (7), Gen-inertia, PGR, and frequency nadir estimated using the proposed FNM in Case II. The scheduling period of the pumping load shifted from midnight to daytime because many PVs were connected to the power system during the daytime. Because of this change, the total PFR and pumping load was considerably lower than that in the nighttime for Case I. Moreover, the frequency nadir could easily fall below 59.5 Hz. We also found that PGRs exceeded 1.6% in all off-peak periods (1:00–8:00). Such a large PGR

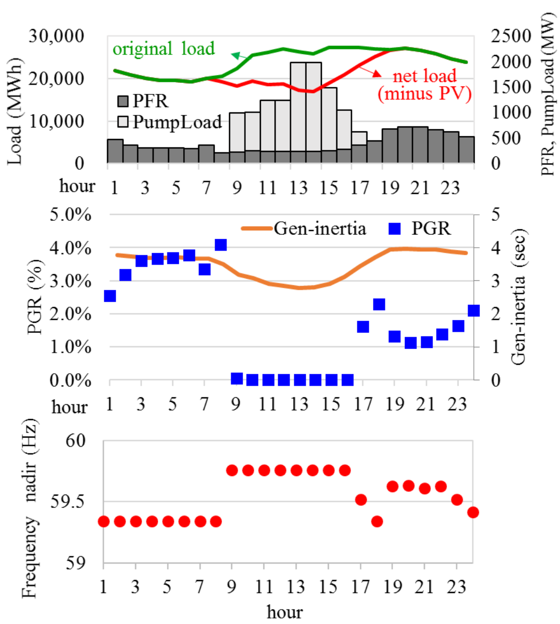

FIGURE 17. Loads, PFRs, PGRs, gen-inertias, and nadir frequencies in each hour estimated using the proposed FNM.

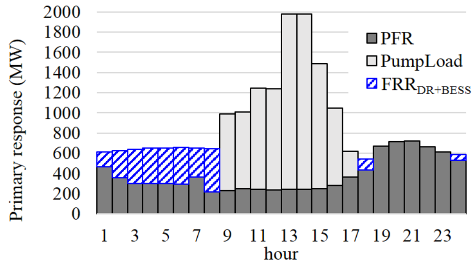

FIGURE 18. FRR capacities at the safe frequency nadir (high PV penetration).

was predicted only using the FNMXGB which learned from the cases with larger frequency deviations.

Fig. 18 summarizes the preparation of the PFR, PumpLoad (pumping load), and $FRR_{DR+BESS}$ that maintains the frequency nadir above 59.5 Hz. $FRR_{DR+BESS}$ must usually be procured during the off-peak periods (first eight hours of the day) because the pumping load has shifted to the daytime. The total capacity of $FRR_{DR+BESS}$ that should be procured over 24 h was 2694 MWh. Comparing the results with those of Case I under the same load demands, Case II requires additional $FRR_{DR+BESS}$ to ensure frequency security.

VII. CONCLUSION

An adequate FRR can avoid UFLS triggering by the frequency below 59.5 Hz after the largest unit trip. The supervised learning algorithm identifies the important key features for constructing the FNM and evaluating the frequency nadir. In the frequency nadir predictions, the FNMXGB developed using the supervised learning technique outperformed the FNMs derived using the conventional swing equation and NN framework. As the frequency nadir can be calculated with a high confidence, additional FRR procurement can be effectively evaluated based on day-ahead unit commitment scheduling. The approach is evaluated in two case studies: one with low RES penetration and the other with high RES penetration. In the first case, the FNM model predicts that the additional FRR capacity must be prepared during the daytime and load-falling period. In the second case, the FNM model predicts that the additional FRR should be prepared during the off-peak hours (from midnight to late morning).

The proposed FNM is still being tested and more information is being gathered. Iterative testing can improve the model's ability to capture the true frequency response of the TPC system, as its generation is transforming into a higher renewable portfolio in the future.

ACKNOWLEDGMENT

The authors thank the anonymous reviewers for their helpful comments.

REFERENCES

[1] E. Ela, M. Milligan, and B. Kirby, "Operating reserves and variable generation," Nat. Renew. Energy Lab., Golden, Colorado, Tech. Rep. TP-5500-51978, Aug. 2011.

[2] *NERC Reliability Standard BAL-001-1-Real Power Balancing Control Performance*. Accessed: Apr. 10, 2021. [Online]. Available: http://www.nerc.com/pa/Stand/Reliability%20Standards/BAL-001-1.pdf

[3] (Apr. 1, 2005). *NERC Reliability Standard BAL-002-0-Disturbance Control Performance*. Accessed: Apr. 1, 2005. [Online]. Available: https://www.nerc.com/files/BAL-002-0.pdf

[4] C. Seneviratne and C. Ozansoy, "Frequency response due to a large generator loss with the increasing penetration of wind/PV generation—A literature review," *Renew. Sustain. Energy Rev.*, vol. 57, pp. 659–668, May 2016.

[5] P. Du, N. V. Mago, W. Li, S. Sharma, Q. Hu, and T. Ding, "New ancillary service market for ERCOT," *IEEE Access*, vol. 8, pp. 178391–178401, 2020.

[6] H. Gu, R. Yan, and T. Saha, "Review of system strength and inertia requirements for the national electricity market of Australia," *CSEE J. Power Energy Syst.*, vol. 5, no. 3, pp. 295–305, Sep. 2019.

[7] D. Fernández-Muñoz, J. I. Pérez-Díaz, I. Guisández, M. Chazarra, and Á. Fernández-Espina, "Fast frequency control ancillary services: An international review," *Renew. Sustain. Energy Rev.*, vol. 120, Mar. 2020, Art. no. 109662.

[8] L. Su, X. Qin, S. Zhang, Y. Zhang, Y. Jiang, and Y. Han, "Fast frequency response of inverter-based resources and its impact on system frequency characteristics," *Global Energy Interconnection*, vol. 3, no. 5, pp. 475–485, Oct. 2020.

[9] E. Pusceddu, B. Zakeri, and G. C. Gissey, "Synergies between energy arbitrage and fast frequency response for battery energy storage systems," *Appl. Energy*, vol. 283, Feb. 2021, Art. no. 116274.

[10] S. P. Melo, U. Brand, T. Vogt, J. S. Telle, F. Schuldt, and K. V. Maydell, "Primary frequency control provided by hybrid battery storage and power-to-heat system," *Appl. Energy*, vols. 233–234, pp. 220–231, Jan. 2019.

[11] P. Babahajiani, Q. Shafiee, and H. Bevrani, "Intelligent demand response contribution in frequency control of multi-area power systems," *IEEE Trans. Smart Grid*, vol. 9, no. 2, pp. 1282–1291, Mar. 2018.

[12] C.-Y. Lai and C.-W. Liu, "A scheme to mitigate generation trip events by ancillary services considering minimal actions of UFLS," *IEEE Trans. Power Syst.*, vol. 35, no. 6, pp. 4815–4823, Nov. 2020.

[13] M. Peydayesh and R. Baldick, "Simplified model of ERCOT frequency response validated and tuned using PMUs data," *IEEE Trans. Smart Grid*, vol. 9, no. 6, pp. 6666–6673, Nov. 2018.

[14] W. Wang, W. Yao, C. Chen, X. Deng, and Y. Liu, "Fast and accurate frequency response estimation for large power system disturbances using second derivative of frequency data," *IEEE Trans. Power Syst.*, vol. 35, no. 3, pp. 2483–2486, May 2020.

[15] (Jun. 4, 2019). *NERC Reliability Guideline Primary Frequency Control*. Accessed: Apr. 10, 2021. [Online]. Available: https://www.nerc.com/comm/OC/RS_GOP_Survey_DL/PFC_Reliability_Guideline_rev20190501_v2_final.pdf

[16] H. Huang and F. Li, "Sensitivity analysis of load-damping characteristic in power system frequency regulation," *IEEE Trans. Power Syst.*, vol. 28, no. 2, pp. 1324–1335, May 2013.

[17] D. del Giudice, A. Brambilla, S. Grillo, and F. Bizzarri, "Effects of inertia, load damping and dead-bands on frequency histograms and frequency control of power systems," *Int. J. Electr. Power Energy Syst.*, vol. 129, Jul. 2021, Art. no. 106842.

[18] C. C. Wu and N. Chen, "Frequency-based method for fast-response reserve dispatch in isolated power systems," *IEE Proc.-Gener., Transmiss. Distrib.*, vol. 151, no. 1, pp. 73–77, Jan. 2004.

[19] R.-F. Chang, C.-N. Lu, and T.-Y. Hsiao, "Prediction of frequency response after generator outage using regression tree," *IEEE Trans. Power Syst.*, vol. 20, no. 4, pp. 2146–2147, Nov. 2005.

[20] L. Wu, S. You, J. Dong, Y. Liu, and T. Bilke, "Multiple linear regression based disturbance magnitude estimations for bulk power systems," in *Proc. IEEE Power Energy Soc. Gen. Meeting (PESGM)*, Portland, OR, USA, Aug. 2018, pp. 1–5.

[21] D. Zografos, T. Rabuzin, M. Ghandhari, and R. Eriksson, "Prediction of frequency nadir by employing a neural network approach," in *Proc. IEEE PES Innov. Smart Grid Technol. Conf. Eur. (ISGT-Europe)*, Sarajevo, Bosnia Herzegovina, Oct. 2018, pp. 1–6.

[22] M. S. Ibrahim, W. Dong, and Q. Yang, "Machine learning driven smart electric power systems: Current trends and new perspectives," *Appl. Energy*, vol. 272, Aug. 2020, Art. no. 115237.

[23] O. A. Alimi, K. Ouahada, and A. M. Abu-Mahfouz, "A review of machine learning approaches to power system security and stability," *IEEE Access*, vol. 8, pp. 113512–113531, 2020.

[24] L. Duchesne, E. Karangelos, and L. Wehenkel, "Recent developments in machine learning for energy systems reliability management," *Proc. IEEE*, vol. 108, no. 9, pp. 1656–1676, Sep. 2020.

[25] H.-W. Chiu, L.-R. Chang-Chien, and C.-C. Wu, "Construction of a frequency compliant unit commitment framework using an ensemble learning technique," *Energies*, vol. 14, no. 2, p. 310, Jan. 2021.

[26] H. Haes Alhelou, M. E. Hamedani Golshan, T. C. Njenda, and N. D. Hatziargyriou, "An overview of UFLS in conventional, modern, and future smart power systems: Challenges and opportunities," *Electr. Power Syst. Res.*, vol. 179, Feb. 2020, Art. no. 106054.

[27] S.-J. Huang and C.-C. Huang, "An automatic load shedding scheme including pumped-storage units," *IEEE Trans. Energy Convers.*, vol. 15, no. 4, pp. 427–432, Dec. 2000.

[28] C.-C. Wu, W.-J. Lee, C.-L. Cheng, and H.-W. Lan, "Role and value of pumped storage units in an ancillary services market for isolated power Systems–Simulation in the taiwan power system," in *Proc. IEEE/IAS Ind. Commercial Power Syst. Tech. Conf.*, Edmonton, AB, Canada, May 2007, pp. 1–6.

[29] B. Ratner, "The correlation coefficient: Its values range between $+1/-1$, or do they?" *J. Targeting Meas. Anal. Marketing*, vol. 17, pp. 139–142, May 2009.

[30] (Feb. 1, 2010). *Scikit-Learn*. Accessed: Apr. 10, 2021. [Online]. Available: https://scikit-learn.org/stable/

[31] S. Badillo, "An introduction to machine learning," *Clin. Pharmacol. Ther.*, vol. 107, no. 4, pp. 871–885, 2020.

[32] J. H. Friedman, "Greedy function approximation: A gradient boosting machine," *Ann. Statist.*, vol. 29, no. 5, pp. 1189–1232, Oct. 2001.

[33] T. Chen, T. He, and M. Benesty, "Xgboost: Extreme gradient boosting," *R Package Version*, vol. 2, pp. 1–4, Aug. 2015.

[34] Y. Yu, X. Si, C. Hu, and Z. Jianxun, "A review of recurrent neural networks: LSTM cells and network architectures," *Neural Comput.*, vol. 31, no. 7, pp. 1235–1270, 2019.

[35] O. Sagi and L. Rokach, "Ensemble learning: A survey," *WIREs Data Mining Knowl. Discovery*, vol. 8, no. 4, pp. 1–18, Jul. 2018.

[36] C. S. Bojer and J. P. Meldgaard, "Kaggle forecasting competitions: An overlooked learning opportunity," *Int. J. Forecast*, vol. 37, no. 2, 2020, Art. no. 587603.

HSIN-WEI CHIU (Student Member, IEEE) received the B.S. degree in electrical engineering from Yuan Ze University, Taoyuan, Taiwan, in 2011, and the M.S. degree in electrical engineering from the National Taiwan University of Science and Technology, Taipei, Taiwan, in 2013. He is currently pursuing the Ph.D. degree in electrical engineering with National Cheng Kung University, Tainan, Taiwan. His research interests include data science, mathematical modeling, and power system operation.

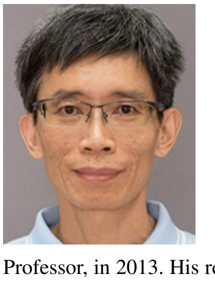

LE-REN CHANG-CHIEN (Senior Member, IEEE) received the B.S. degree in engineering science from National Cheng Kung University, Tainan, Taiwan, in 1993, the M.S.E.E. degree from the University of Wisconsin-Madison, Madison, WI, USA, in 1998, and the Ph.D. degree from Purdue University, West Lafayette, IN, USA, in 2002. He joined the Department of Electrical Engineering, National Cheng Kung University, as an Assistant Professor, in 2003, where he became a Professor, in 2013. His research interests include power electronics, renewable energy applications, power system operation, control, and reliability.